International Journal of Hydrogen Energy 138 (2025) 1057–1065

Contents lists available at ScienceDirect

International Journal of Hydrogen Energy

journal homepage: www.elsevier.com/locate/he

Influence of 1-propanol/water ratio in catalyst inks for doctor-blade coated H_2-PEMFC electrodes

Marc Ayoub [a,b], Christoph Hübner [a,b], Philipp Martschin [a,b], Jochen Kerres [a,c], Simon Thiele [a,b], Matthew Brodt [a,*]

[a] Helmholtz-Institute Erlangen-Nürnberg for Renewable Energy (IET-2), Forschungszentrum Jülich, Cauerstr. 1, 91058, Erlangen, Germany
[b] Department of Chemical and Biological Engineering, Friedrich-Alexander-Universität Erlangen-Nürnberg, Cauerstr. 1, 91058, Erlangen, Germany
[c] Chemical Resource Beneficiation Faculty of Natural Sciences, North-West University, Potchefstroom, 2520, South Africa

ARTICLE INFO

Handling Editor: Søren Juhl Andreasen

ABSTRACT

In this study, we vary the 1-propanol/water and ionomer/carbon (I/C) ratios in catalyst inks with a high total solid content of 10 wt%. The influence of the ratios on the inks is analyzed via the processing properties, while the resulting electrodes are characterized using electrochemical hydrogen fuel cell tests. The 1-propanol/water ratio variation showed a stronger effect on the rheological and wetting properties and thus the coating qualities for low I/C inks than for high I/C inks. Different void volume fractions and electrode thicknesses are observed for the various ionomer contents and alcohol concentrations for the coated electrodes. In some cases, primarily in low I/C inks, significant differences in proton conduction and mass transport properties are observed by detailed electrochemical analysis. For some ink formulations these differences counterbalance each other, resulting in minimal net differences in the polarization curves. As a result, the interplay between ionomer concentration and alcohol content is shown to be non-straightforward and significant for optimizing the formulations of high solid weight content inks.

1. Introduction

The formulation of catalyst inks is an indispensable step for fabricating electrodes for hydrogen proton exchange membrane fuel cells (H_2-PEMFCs). Inks are usually composed of catalysts, solvents, and ionomer dispersions. Solid weight contents (wt%) for inks vary across literature and are usually adjusted to meet the coating techniques' requirements. Nevertheless, the inks are often dispersed in mixtures of water and alcohol (e.g. 1-propanol or 2-propanol) as solvents [1–3]. Similarly, ionomer dispersions are often dispersed in mixtures of alcohol and water. For high ionomer concentrations in dispersions, increasing alcohol contents have been reported to increase backbone swelling, chain clustering (electrostatic interactions between SO_3^- and H_3O^+), and aggregate sizes [4–6]. Likewise, for inks, different alcohol contents have been reported to affect aggregate sizes, pore structures, and the distribution of ionomers in catalyst layers [1,7–10]. For example, for colloidal systems with low solid weight contents, a higher water-to-alcohol ratio (1-propanol or 2-propanol) has often been reported to result in better electrochemical performances attributed to better mass transport properties, ionomer catalyst interfaces, and catalyst activities [7, 10–13]. However, the trend for higher solid weight contents is not entirely clear. For example, a recent study investigated the influences of 12 different solvents for screen-printing [14]. Various solvents such as DI-water, ethanol, butanol, and 1,2-propanediol were investigated with evaporation, sedimentation, rheological, and contact angle experiments. However, a clear trend between solvent, dielectric constants, and fuel cell performances could not be observed due to the complex interactions within the systems [14]. Also, different evaporation rates and drying mechanisms could have led to morphological differences despite similar dielectric constants [14,15]. A molecular dynamics study of different solvents and 20 wt% ionomers (equivalent weights (EWs) of 760, 1140, and 1560) with graphite sheets showed that the amount of ionomer adsorbed on the graphite surface is strongly influenced by the EW and alcohol content [16]. For low EWs, the maximum ionomer coverage was observed for water-rich solvents, whereas for high EWs, high alcohol contents were necessary for enhanced adsorption [16]. In another project, collaborators observed that the 1-propanol mole fraction in inks and the ionomer-to-carbon (I/C) ratio (EW 1000) had a substantial

* Corresponding author.
E-mail address: ma.brodt@fz-juelich.de (M. Brodt).

https://doi.org/10.1016/j.ijhydene.2025.05.107
Received 23 March 2025; Received in revised form 5 May 2025; Accepted 8 May 2025
Available online 22 May 2025

impact on the crack formation of gas diffusion electrodes (GDEs) [17,18]. Fewer crack formations were observed for i) higher I/Cs and ii) 1-propanol mole fractions of 0.5 whereas both higher and lower alcohol fractions resulted in more visible cracks. Preliminary results indicated that higher water contents in inks for slot-die coated GDEs resulted in better fuel cell performance and that the least-cracked catalyst layers had lower initial performance. However, a causal relationship was not established [17]. In another study, slot-die and gravure-coated inks with 4.7 wt% (EW 1000) showed better electrochemical properties for water-rich inks and different ionomer concentrations in the through-plane direction of the electrodes [19]. In a separate investigation, variations for 1-propanol and 2-propanol with water mixtures were made for mayer rod coating inks with I/Cs of 0.65 and weight contents of >10 wt% [1]. The water content was varied between 16 and 65 wt% for the solvents, and the ionomer had an EW of 700 g mol^{-1}. Among the findings is that the decal transfer for the electrode with 65 wt% water in 2-propanol had a poor transfer to the membrane due to poor ionomer distribution in the electrode [1]. Also, the best performance at two different operating conditions was observed for the sample with 16 wt% H_2O in 1-propanol. Potentially, ionomer patches present with high water contents hindered oxygen transport in macropores due to more coverage of the electrode's upper surface [1].

Despite the vast literature using different solvents and solid weight contents for catalyst inks, a precise understanding of their impact on electrochemical performance is still unclear. Different trends for dispersions with different alcohol and solid weight contents have been observed for bulk properties such as viscosity [4,20–22]. A similar scenario might apply to catalyst inks. With that in mind, the present study further investigates high solid weight content inks (10 wt%) and explores how alcohol and ionomer contents impact coating qualities and electrochemical performances. Ultimately, valuable insights are highlighted for the complex behavior of high solid weight content catalyst inks.

2. Experimental

2.1. Ink preparation

A 3 M™ dispersion was formulated using a short-sided chain (SSC) ionomer with an EW of ~800 g mol^{-1}. First, 60 wt% of anhydrous 1-propanol was added to the ionomer, allowing it to swell for 2 h on a heating plate preset at 80 °C ($T_{internal}$ measured around 50 °C) with a stirring speed of 500 RPM. Afterward, 40 wt% of ultrapure water (18.2 MΩ cm resistivity) was added, and the mixture was allowed to homogenize for 3 days. The dispersion was then heated to 120 °C ($T_{internal}$ measured around 70 °C) for 1 h before cooling to room temperature. Finally, the dispersion was left to rest for one additional day, and the final solid weight content was quantified to be 22 wt%.

A 30 wt% Pt/C catalyst (Tanaka®, TEC10V30E) was used to make six different inks with three different alcohol contents and a fixed solid weight content (Pt/C + dry ionomer) of 10 wt%. The three alcohol contents were, respectively, 30 wt% (1-Prop 30 %), 60 wt% (1-Prop 60 %), and 80 wt% of 1-propanol (1-Prop 80 %), with the balance of water for the remaining total solvent. Two different inks with I/Cs of ~0.72 and ~1.07 defined by mass were made for each alcohol content. All inks were prepared by first weighing ~500 mg of catalyst, followed by water, and then physically mixing the 15 mL HDPE bottle by hand. Afterward, 1-propanol was added to the catalyst followed by the ionomer dispersion. The inks were then roller mixed (Ratek Roler mixer- BTR5- 12V) for ≈18 h at ~22 °C. The HDPE bottles were rotating at 60 RPM and contained ≈17 g/bottle of 5 mm ZrO_2 beads for mixing.

2.2. Electrode and cell manufacturing

Doctor-blade (Proceq ZUA 2000.100) coatings on virginal PTFE decal sheets (~50 μm thick) were made at 100 mm s^{-1} on a 60 °C coating table (Coatmaster 510, Erichsen) with active vacuum suction. The measured relative humidity (RH) was 60–70 %, and the wet film thicknesses were 275 μm for I/C ratios of 0.72 and 300 μm for I/C 1.07. The shear rates during coating were therefore 333 s^{-1} and 364 s^{-1} for the I/C ratios of 0.72 and 1.07 respectively. After coating, the electrodes were annealed at 180 °C for 10 min per the ionomer manufacturer's recommendation. All anodes used had I/Cs of 0.72 (1-Prop 60 %) and Pt loadings of 0.333 ± 0.038 $mg_{Pt}{\cdot}cm^{-2}$. The cathode platinum loadings for I/C ratios of 0.72 were for 1-Prop 30 %, 1-Prop 60 %, and 1-Prop 80 %, respectively 0.338 ± 0.012, 0.346 ± 0.015, and 0.317 ± 0.007 $mg_{Pt}{\cdot}cm^{-2}$. For I/Cs of 1.07, the loadings were 0.320 ± 0.006, 0.309 ± 0.008, and 0.298 ± 0.008 $mg_{Pt}{\cdot}cm^{-2}$, respectively for the 1-Prop 30 %, 1-Prop 60 %, and 1-Prop 80 % inks. Electrodes in 5 cm^2 areas were stamped out and hotpressed on 25 cm^2 Nafion™ 211 membranes as previously reported, forming decal-transferred catalyst-coated membranes (CCMs) [23]. Hotpressing was performed by first conditioning the sample for 60 s at 120 °C and 0.5 MPa. Then, the temperature was ramped to 155 °C in 150 s, and the pressure increased to 1.2 MPa for 240 s. For all CCMs, a total decal transfer was achieved regardless of the alcohol content in the inks.

2.3. Ex situ analysis

The viscosity of the inks was screened using a HAAKE™ MARS™ 40 Rheometer with a C60 0.5°/Ti cone set at 22 °C using a Peltier cooling/heating option. The inks were first transported to the rheometer and left to rest for 5 min before slowly pipetting 500 μL samples. No bubbles were observed during the pipetting process, and each measurement was repeated three times. For the measurements, 50 linear steps were made between shear rates of 10 s^{-1} and 500 s^{-1}, while holding each step for 10 s to ensure a steady state response. Then, the shear rate was held for 3 additional seconds to get an average viscosity response.

Contact angle measurements of the inks were made using a drop shape analyzer (DSA30) from Krüss with their default ADVANCE software. The sessile drop method was used with an automatic baseline and tangent fitting method for the left and right contact angles. Droplets were dosed on virgin decal sheets, and the contact angles were measured directly after deposition, after 30 s, then 60 s, and finally after 90 s.

Coated electrodes were screened for irregularities using a Canon EOS 6D camera with ISO set to Auto, a shutter speed of 1:4000, an aperture of F/2.8, and a Tamron SP 90 mm F/2.8 Ø58 Macro 1:1 VC USD objective/lens. The coated decal sheets were placed on a Dörr LT-2020 LED lighting tablet set at maximum white lighting. These images can be found in the supplementary information. In addition to the above visualization, scanning electron microscopy (SEM) images of cross-sectionally embedded membrane electrode assemblies (MEAs) were made as described previously [23].

2.4. Electrochemical analysis

Each alcohol and I/C ratio was tested three times (three MEAs) using an automated protocol at a commercial 850g FC testing system (Scribner Associates Inc.) and a VSP-300 (BioLogic) potentiostat. Freudenberg gas diffusion layers (5 cm^2 H14CX483) were compressed by 25 ± 1 % using glass-fiber-reinforced PTFE gaskets, and a commercial 5 cm^2 cell fixture with a torque of 5 N m was used as before [23].

Linear sweep voltammetry (LSV) measurements were initially made at 100 % RH, 80 °C, and 150 kPa absolute + atmospheric pressures to check for electrical shorts in the membrane and to quantify the hydrogen crossover. An example of an LSV measurement is shown in Fig. S7. During an LSV measurement, the cathode (working electrode) is purged with inert gas like nitrogen, while the anode (counter and reference electrode) with hydrogen. The flow rates were 0.20 L min^{-1} of H_2 and N_2 for the anode and cathode, respectively. The hydrogen crossing through the membrane to the cathode, reacts via the hydrogen oxidation reaction mechanism at positive potentials, generating protons and electrons. On

the anode the hydrogen evolution reaction occurs consuming the generated electrons and protons. As a result, the current flows in the opposite direction. For this study, the LSVs were scanned from ~0.1 V to 0.4 V at 2 mV s^{-1} [24,25].

After the LSVs, the gases were changed to 0.20 L min^{-1} of H_2 for the anode and 0.75 L min^{-1} of air for the cathode at 94 % RH, 80 °C, and 150 kPa absolute. The cells were then broken-in by voltage holds at 0.6 V (20 min) and 0.3 V (20 min) with open circuit voltage (OCV) holds in between (2 min) for 7–10 cycles [26]. Afterward, polarization curve measurements were performed galvanostatically with 10 steps from OCV until 0.100 A cm^{-2} and 13 steps between 0.150 A cm^{-2} and 2.200 A cm^{-2}. The flow rates were kept fixed at 0.20 L min^{-1} of H_2 for the anode and 0.75 L min^{-1} of air for the cathode, resulting in a theoretical maximum current density of 5.74 A cm^{-2} at STP conditions assuming 100 % faradaic efficiency. Each current step was maintained for 2 min, during which the last 30 s were averaged for the voltage response. At each step, a galvanostatic impedance measurement was made from 100 kHz to 1 Hz with 10 % amplitude and 10 points per decade. The high frequency resistances (HFRs) were quantified by fitting impedance plots between 30 kHz and 100 Hz [27,28].

Protonic sheet resistances were quantified using six measurements of one representative MEA per I/C ratio per alcohol content [23]. Flow rates were 0.20 L min^{-1} for H_2 and N_2 on the anode and cathode, respectively, and the voltage was set at 0.2 V to ensure blocking conditions. An amplitude of 10 mV was used, and the frequency was swept between 500 kHz and 0.2 Hz, with 10 points per decade and 5 average measurements per frequency. For analysis, the highest frequency was limited to 30 kHz, and the spectra were fitted using the "Z-Fit" function in EC-Lab software with the "Randomize + Simplex" method [29–31].

For one representative MEA per I/C ratio per alcohol content, limiting current experiments were conducted at atmospheric, 150 kPa, 200 kPa, and 300 kPa absolute pressures. The oxygen concentrations on the cathode were 3 vol%, 3.5 vol%, 4 vol%, and 5 vol% in N_2 with a total flow rate of 0.95 L min^{-1}, and 0.20 L min^{-1} of H_2 on the anode. The voltage was stepwise-varied from 0.5 V to 0.1 V ($\Delta V = 0.1$ V) and then from 0.07 V to 0.05 V ($\Delta V = 0.01$ V) while holding each step for 1 min and averaging the last 30 s for the current response. Limiting currents were determined at 0.07 V to quantify the total mass transport resistance, $R_{T,O2}$. The total mass transport resistance was split into pressure-dependent, $R_{PD,O2}$, and pressure-independent, $R_{PI,O2}$, parts as described by Baker et al. $R_{T,O2} = R_{PD,O2} + R_{PI,O2}$ [32].

The above mentioned measurements, excluding LSV, were repeated under symmetric RHs of 60 %, 30 %, and 15 %. An additional measurement was also made under asymmetric conditions with 15 % RH on the anode and a dry cathode. However, at symmetric 15 % RH and under the asymetric conditions no clear differences could be observed due to the high resistance of the system (e.g. high HFR). Consequently, the data could not be accurately processed under these conditions and the results were omitted. After changing the RH, the cell was reconditioned by short voltage holds between 0.6 V (5 min) and 0.3 V (5 min) with OCV in between (30 s).

Finally, the electrochemically active surface area (ECSA, $m^2 \cdot g^{-1}$) was quantified by three cyclic voltammetry (CV) measurements at 40 °C, atmospheric pressure, and 100 % RH. The voltage was swept with 100 mV s^{-1} from 0.03 V to 0.6 V with 0.2 L min^{-1} of 5 % H_2 in N_2 on the anode and 0 L min^{-1} on the cathode after N_2 purging. The ECSA was determined between 0.06 V and 0.40 V from the q_{HUPD} region, assuming a 210 μC cm^{-2} adsorption charge of Pt, Fig. S6 [25].

3. Results and discussion

3.1. Rheology and contact angle

For clarity, the following abbreviations are used for the discussion: For inks with a solvent composition of 30 wt% 1-propanol and the balance water: 1-Prop 30 % (—▲—) I/C 0.72 and 1-Prop 30 % (—△—) I/C 1.07. Similarly, for inks with 60 wt% of 1-propanol, we use 1-Prop 60 % (—▼—) I/C 0.72 and 1-Prop 60 % (—▽—) I/C 1.07 and for inks with 80 wt % of 1-propanol we use 1-Prop 80 % (—◆—) I/C 0.72 and 1-Prop 80 % (—◇—) I/C 1.07. Fig. 1a and b highlight the influence of the alcohol content on the viscosity profile for inks with I/C ratios of 0.72 and 1.07, respectively. For I/C of 0.72, Fig. 1a, inks with 1-Prop 30 % (—▲—) and 1-Prop 60 % (—▼—) show overlapping behaviors at both low and high shear rates. On the other hand, inks with 1-Prop 80 % (—◆—) show lower viscosities at low shear rates but still approach the same viscosity values as the lower alcohol content inks at high shear rates, which is relevant for coating processes. For I/Cs of 1.07, Fig. 1b, the alcohol content is found to have little influence on the measured viscosities since an overlapping behavior is observed at all shear rates while noting the error-bars. In Fig. 1c, a comparison between the I/C ratios is done for 1-Prop 60 %. As depicted, inks with I/Cs of 1.07 show lower viscosities compared to inks with I/Cs of 0.72. A similar trend is also observed for the other samples with the regions where the shear rates overlap varying among the different alcohol contents, Fig. S8. The lower viscosities for inks with I/Cs of 1.07 are attributed to more ionomer adsorption on the catalyst, enhancing electrostatic repulsion while shielding carbon-carbon attractive forces [16,33].

Fig. 2a and b show measured contact angle values for inks with I/Cs of 0.72 and 1.07, respectively. At an I/C of 0.72, inks with a higher alcohol content had lower contact angles and thus better wetting behavior on the decal foils. In particular, the ink with the lowest alcohol content tested, 1-Prop 30 % (—▲—) I/C 0.72, had both a much higher initial contact angle than the 60 % and 80 % alcohol inks as well as less of a decrease in contact angle over 90 s. On the other hand, the inks with I/Cs of 1.07 had contact angle profiles that were less impacted by the water-alcohol ratio. Also, measured values for 1-Prop 80 % (—◆—) I/C 0.72 were only slightly higher than 1-Prop 80 % (—◇—) I/C 1.07. As a result, only minor wetting differences are observed due to the more hydrophobic nature of the inks despite the different I/C ratios. This suggests that inks with either higher alcohol or ionomer contents with favored hydrophobic interactions can result in better wetting behaviors, as shown in the next section.

3.2. Cross-sectional images and coating qualities

Fig. 3 shows representative cross-sectional images of the tested MEAs from coated electrodes. The remaining images can be found in Fig. S2 and S3 with a summary of physical properties in Table S1.

It is clear from Fig. 3a that an I/C ratio of 0.72 with 1-Prop 30 % resulted in structural discontinuities; notable inhomogeneities are marked with red circles. This result is perhaps not surprising as the contact angle measurements and the camera pictures in Fig. S1 both also resulted in worse results for this ink. Interestingly, the worse quality is not reflected in the viscosity measurements (Fig. 1a) since the rheological profiles for 1-Prop 30 % (—▲—) I/C 0.72 and 1-Prop 60 % (—▼—) I/C 0.72 overlapped.

In general the higher I/C ratios resulted in thinner electrodes, with the exception being at low alcohol content, where there is no/less difference visible in Fig. 4 and Table S1. To rule out processing contributions to the thicknesses, such as from hotpressing, non-hotpressed electrodes on decal sheets were also embedded and found to have similar thicknesses as the hotpressed ones (Fig. S3). These results suggest that the properties of the inks can influence the packing densities and electrode thicknesses, which in turn can result in different void volume fractions (Table S1). The reason for this behavior is not clear. However, one can speculate that a change in alcohol and water contents could have led to different ionomer structures as reported in various studies [6,34–37]. These could have led to different catalyst-ionomer and ionomer-ionomer interaction strengths, which with more alcohol favor ionomer entanglement through the more mobile hydrophobic backbones. As a result, at higher I/Cs and high alcohol contents, more ionomer entanglement could have led to more compact packing during

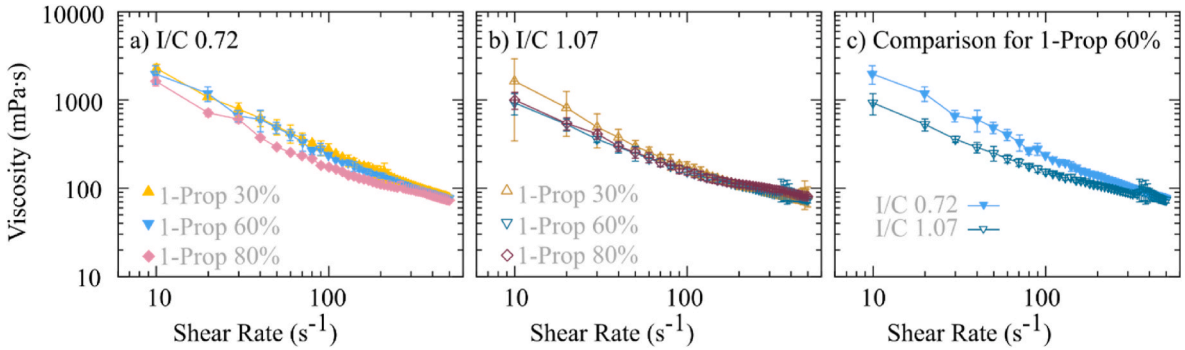

Fig. 1. Viscosity measurements of the different inks for a) I/C 0.72 for 1-Prop 30 % (▲), 1-Prop 60 % (▼), and 1-Prop 80 % (◆). b) I/C 1.07 for 1-Prop 30 % (△), 1-Prop 60 % (▽), and 1-Prop 80 % (◇). c) Comparison between I/C 0.72 (▼) 1-Prop 60 % and I/C 1.07 (▽) 1-Prop 60 %.

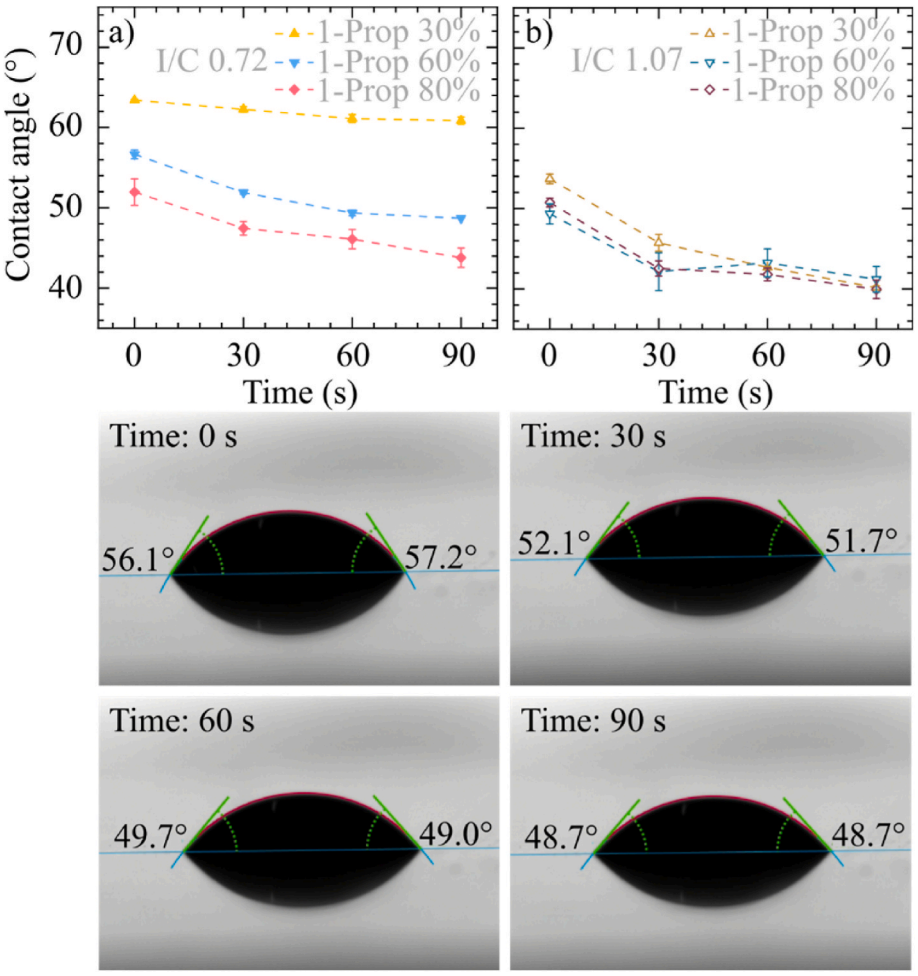

Fig. 2. Measured contact angles for a) I/C ratios of 0.72 for 1-Prop 30 % (▲), 1-Prop 60 % (▼), and 1-Prop 80 % (◆). b) I/C 1.07 for 1-Prop 30 % (△), 1-Prop 60 % (▽), and 1-Prop 80 % (◇). The representative contact angle values at 0 s, 30 s, 60 s, and 90 s are for 1-Prop 60 % (▼) I/C 0.72.

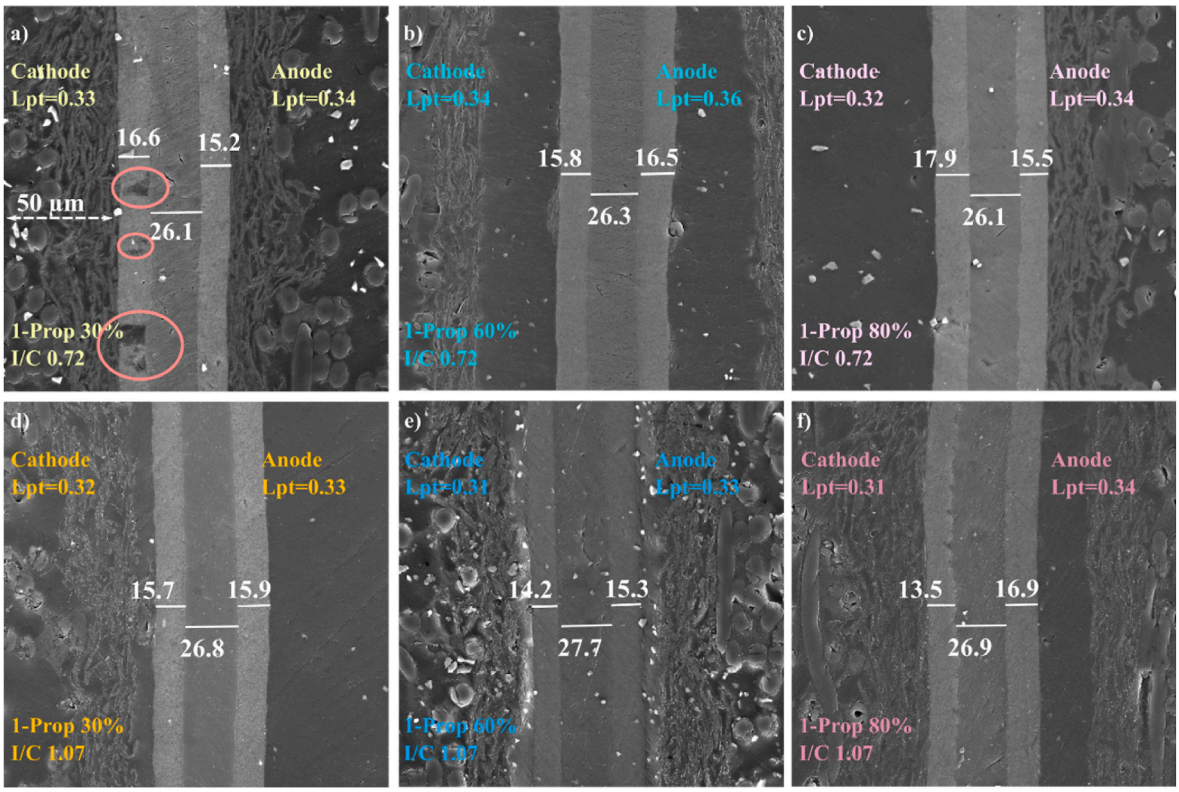

Fig. 3. Cross-sectional images of tested MEAs with images taken at 20.0 kV, a working distance of 5 mm, and a view field of 200 µm. Platinum loadings are given in the top of each image (in mg_{Pt} cm^{-2}), and thicknesses are given in the center of the images based on at least 15 measurements per given thickness (in µm). Inhomogeneities are marked with a light red circle. (For interpretation of the references to colour in this figure legend, the reader is referred to the Web version of this article.)

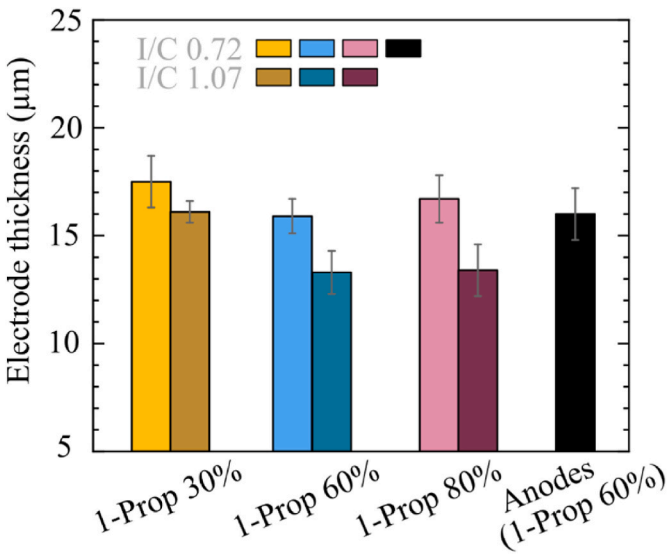

Fig. 4. Overall electrode thicknesses for I/C 0.72, 1-Prop 30 % (▬), 1-Prop 60 % (▬), and 1-Prop 80 % (▬), anodes with 1-Prop 60 % (▬); I/C 1.07, 1-Prop 30 % (▬), 1-Prop 60 % (▬), and 1-Prop 80 % (▬).

film formation and consequently thinner electrodes, whereas at low alcohol contents this effect is minimized. Another possible explanation for this behavior is related to the better wettability at higher alcohol contents which could have led to a denser structure. Different agglomerate sizes could also have led to the observed differences. For now, the exact reason for this behavior remains unknown.

3.3. Electrochemical results

The protonic sheet resistances of the catalyst layers and their protonic conductivities corresponding to the electrodes' thicknesses can be seen in Fig. 5a and Fig. 5b, respectively. For all alcohol contents, higher I/C ratios resulted in better conductivities. It is also evident that the inhomogeneously coated sample with 1-Prop 30 % (—▲—) I/C 0.72 had the poorest conductivities and the highest resistances at all RHs. Among the inks with I/Cs of 1.07, 1-Prop 30 % (—△—) also had the poorest conduction properties. However, the observed differences for 1-Prop 30 % (—▲—) I/C 0.72 are bigger than those of 1-Prop 30 % (—△—) I/C 1.07. This suggests that low alcohol contents result in morphologies that are less effective for proton transfer, with the poorer conductivity being stronger expressed at low ionomer contents.

The mass transport properties were evaluated at 30 % RH, representing a stable RH without extreme mass transport or proton conduction limitations. The total mass transport resistances, $R_{T,O2}$, can be seen in Fig. 6a. The contributions of pressure-dependent, $R_{PD,O2}$, and independent, $R_{PI,O2}$, resistances can be seen in Fig. 6b, for 50 kPa gauge.

Analyzing Fig. 6a, one notices that all measured samples had a linear increase of $R_{T,O2}$ with increasing pressure, indicating valid limiting current measurements. However, slight differences are observed for $R_{T,O2}$, which when measured at different pressures resulted in slightly different slopes and y-intercepts. From the slopes and y-intercepts, the pressure dependent and pressure independent terms, $R_{PD,O2}$ and $R_{PI,O2}$,

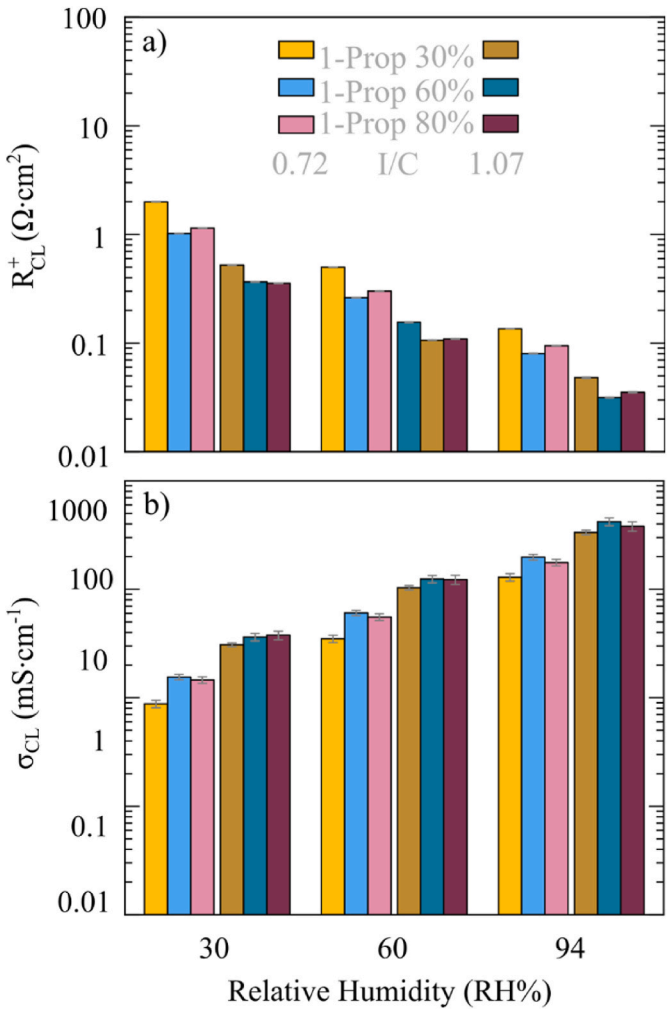

Fig. 5. Impedance measurement results under blocking conditions for MEAs manufactured with electrode inks with various I/C ratios and 1-propanol concentrations. for a) Protonic sheet resistance and b) protonic sheet conduction normalized to the electrode thicknesses, determined at different RHs for I/C 0.72, 1-Prop 30 % (▬), 1-Prop 60 % (▬), and 1-Prop 80 % (▬); I/C 1.07, 1-Prop 30 % (▬), 1-Prop 60 % (▬), and 1-Prop 80 % (▬).

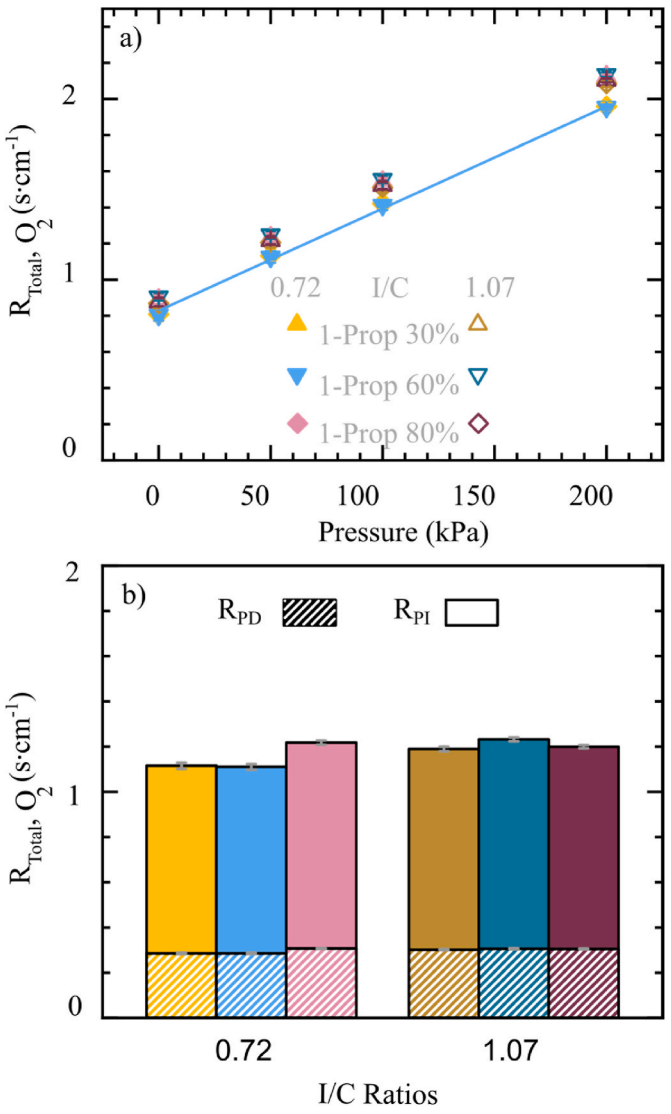

Fig. 6. Total mass transport resistances measured at 80 °C and 30 % RH for one representative sample per I/C ratio per alcohol content with a) showing the total mass transport resistances, $R_{T,O2}$, at different pressures and a linear fit for I/C 0.72, 1-Prop 60 % (▬), b) showing pressure dependent, $R_{PD,O2}$, and pressure independent, $R_{PI,O2}$, components to the total resistances for I/C 0.72, 1-Prop 30 % (▬), 1-Prop 60 % (▬), and 1-Prop 80 % (▬); I/C 1.07, 1-Prop 30 % (▬), 1-Prop 60 % (▬), and 1-Prop 80 % (▬).

were calculated, as shown in Fig. 6b. Comparing the different alcohol contents for I/Cs 0.72, the highest $R_{PI,O2}$ is observed for 1-Prop 80 % (▬), indicating worse Knudsen diffusion processes and/or local O_2 diffusion through ionomer films compared to 1-Prop 30 % (▬) I/C 0.72 and 1-Prop 60 % (▬) I/C 0.72 [32,38,39]. For the higher I/Cs of 1.07, the overall resistances are within error-bars and only slightly higher for 1-Prop 60 % (▬).

The polarization curves and their accompanying HFR data are shown in Fig. 7 at different relative humidities. The HFRs are found to be within error-bars, ruling out different membrane contributions. Only minor differences in the polarization curves are observed for the samples with I/Cs of 0.72, Fig. 7a–c, suggesting that the coating quality is not strongly reflected in the polarization curve measurements. Compared with 1-Prop 60 % (▬) I/C 0.72 and 1-Prop 80 % (▬) I/C 0.72, the ink with 1-Prop 30 % (▬) I/C 0.72 had slightly lower performance at lower RHs due to the higher protonic sheet resistance, Fig. 7c. The protonic sheet resistance is known to be humidity dependent, and the difference in performance for 1-Prop 30 % (▬) I/C 0.72 is, therefore, mostly visible at 30 % RH, in Fig. 7c. At higher relative humidities, Fig. 7a and b, the differences are less distinguishable and a more overlapping behavior is observed between 1-Prop 30 % (▬) and 1-Prop 80 % (▬) I/C 0.72. On the other hand, the slightly lower performance for 1-Prop 80 % (▬) I/C 0.72 compared with 1-Prop 60 % (▬) I/C 0.72 at all RHs is due to the slightly higher mass transport resistance. This is reflected at all relative humidities, and the difference compared with 1-Prop 60 % (▬) I/C 0.72 remains fairly consistent, RH independent. For I/Cs of 1.07, the slightly better mass transport resistance and worse protonic sheet resistance of 1-Prop 30 % (▬) compared to 1-Prop 60 % (▬), lead to counterbalancing effects in the polarization curves, Fig. 7d–f. Similarly, counterbalancing effects for 1-Prop 80 % (▬) I/C 1.07, also led to overlapping performance at all RHs with 1-Prop 30 % (▬) and 1-Prop 60 % (▬).

4. Conclusion

In this study, high solid weight content (10 wt%) electrode inks were manufactured with two different I/C ratios (0.72 and 1.07) and three different 1-propanol/water weight contents (30 wt%, 60 wt% and 80 wt % of 1-propanol). Rheological measurements for I/Cs of 0.72 showed that the inks with a high alcohol content can lead to lower viscosities at

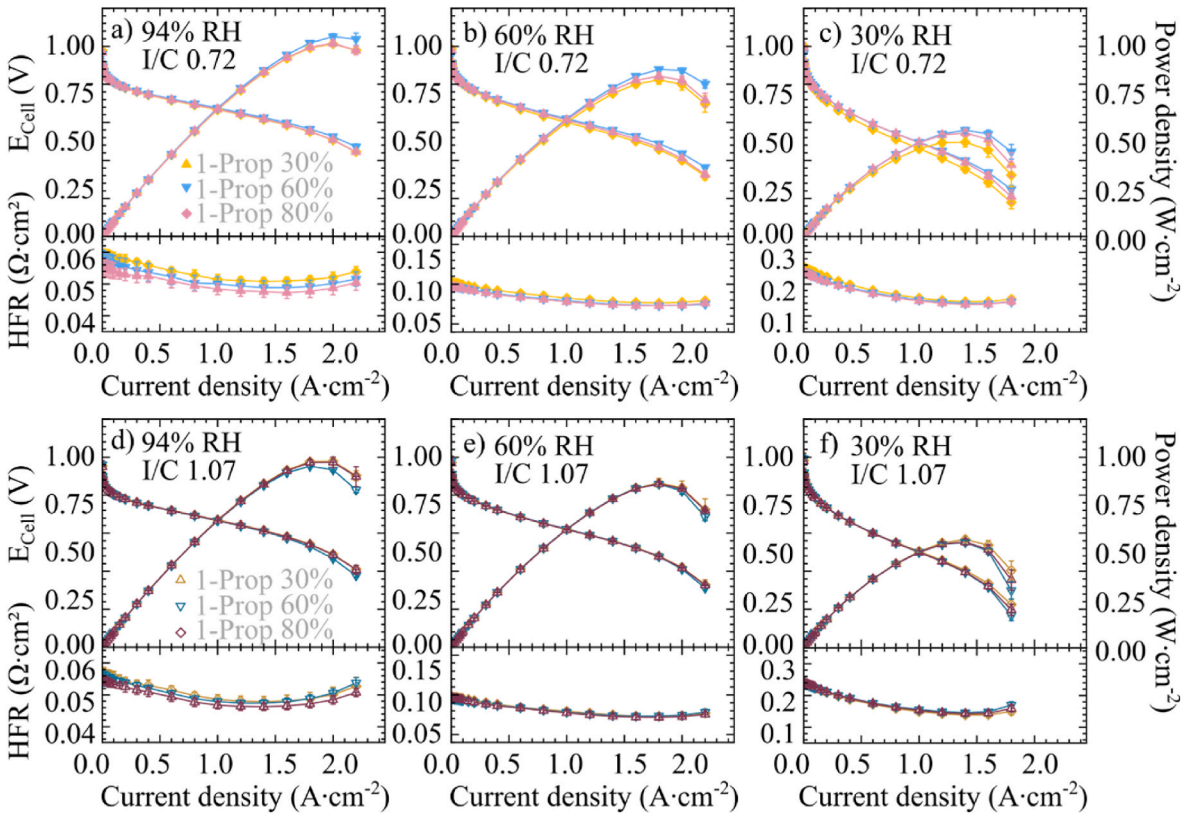

Fig. 7. Performance curves with HFRs based on three different MEAs measured at 80 °C and 50 kPa gauge backpressure for I/Cs of 0.72, 1-Prop 30 % (—▲—), 1-Prop 60 % (—▼—), and 1-Prop 80 % (—◆—) at a) 94 % RH, b) 60 % RH, c) 30 % RH; and I/Cs 1.07 for 1-Prop 30 % (—△—), 1-Prop 60 % (—▽—), and 1-Prop 80 % (—◇—) at d) 94 % RH, e) 60 % RH, f) 30 % RH.

low shear rates which approach similar values at high shear rates. However, the viscosities for higher I/Cs were within error-bars regardless of the shear rate and alcohol content. Contact angle measurements revealed better wetting behaviors for higher alcohol content inks with an I/C of 0.72. At I/Cs of 1.07, the contact angles showed similar values regardless of the alcohol content. The different wetting behaviors also resulted in different coating qualities whereby 1-Prop 30 % I/C 0.72 was the most inhomogeneous. However, this was not directly reflected in the prior viscosity measurements. With SEM cross-sectional analysis of the tested samples, different thicknesses were observed for the different I/C ratios for 1-Prop 60 % and 1-Prop 80 %. Contrarily, 1-Prop 30 % showed similar thicknesses for the different I/C ratios, suggesting that the ink properties can influence the electrodes' morphological structures. The exact reason for this behavior is not clear. However, it is speculated that different degrees of entanglement and interaction strengths for the catalyst-ionomer and ionomer-ionomer systems could have led to the observed differences. Other possible contributing factors can include enhanced wetting properties at high alcohol concentrations and also potentially different aggregate sizes for the different inks. Electrochemical measurements revealed that 1-Prop 30 % (—▲—) I/C 0.72 had a relatively poorer performance at lower RHs due to worse proton conduction properties of the catalyst layers. On the other hand, 1-Prop 80 % (—◆—) I/C 0.72 had worse mass transport properties than the remaining samples. These properties resulted in worse performance than 1-Prop 60 % (—▼—) I/C 0.72, which showed a better balance between mass transport and proton conduction properties. This observation suggests that the worse coating quality for 1-Prop 30 % I/C 0.72, reflected by the worse wetting behavior also results in worse proton conduction, possibly due to a less interconnected catalyst layer. Interestingly, the slightly worse mass transport properties, likely due to impaired Knudsen diffusion and/or local O_2 diffusion through the ionomer films for 1-Prop 80 % I/C 0.72, are not captured by the ex-situ measurements. This suggests that more advanced tools are required to probe in detail the catalyst layer and ionomer-catalyst interfaces, going beyond the standard methods typically employed. For higher I/C ratios, the polarization curves were found to overlap at different RHs. The resistances due to the different mass transport and proton conduction properties balanced each other out, which led to similar performances. However, also for an I/C of 1.07, an ink with 30 % of 1-Prop resulted in worse proton conduction reflected by a thicker electrode compared to 1-Prop 60 % I/C 1.07 and 1-Prop 80 % I/C 1.07. Since the same amount of ionomer was used for the different alcohol contents, a less packed structure is hypothesized to potentially result in worse proton conduction properties, though not always directly reflected in the contact angle measurements and coating quality.

In literature, most studies use one fixed I/C ratio and less concentrated inks. A low alcohol content was often found to result in better performances due to enhanced mass transport properties, ionomer-catalyst interfaces, and catalyst activities [7,10–13]. In this study, we observe that this trend doesn't hold for high solid weight content inks. Moderate to high alcohol contents are found to be favorable for low I/C ratios, similar to another study in the literature [1]. However, in contrast to Ref. [1], the optimal alcohol content is found to be different, possibly due to the different ionomer used and/or drying temperature employed during coating [1]. On the other hand, for higher I/C ratios, the differences in performance are observed to be more subtle compared to available literature due to opposite trends for the mass transport and proton conduction properties. These observations overall suggest that the different alcohol contents cause different ionomer-catalyst and ionomer-ionomer interactions, with their impact being less visible for

higher ionomer concentrations as long as ionomer-catalyst and ionomer-ionomer interactions remain favorable.

In general, it is speculated that low alcohol contents should be avoided for low I/C ratios in concentrated inks when catalyst-ionomer and ionomer-ionomer interactions are unfavorable. Instead, intermediary alcohol contents can be optimal, requiring separate dedicated optimization studies to determine the exact optimal composition. The inks can then be employed for applications operating at high RHs where low I/Cs are regularly used. On the other hand, applications at lower RHs where higher I/Cs are frequently used can benefit from lower alcohol contents, and thus reduce manufacturing costs and the risk of forming explosive mixtures. Naturally, also favorable catalyst-ionomer and ionomer-ionomer interactions are required. Overall, the present investigation highlights the importance of tailoring ink compositions for I/C ratios for optimized morphologies, coatings, and electrochemical performances. Consequently, more systematic investigations are required for future studies to understand the complex interplays at microscopic levels and their impact on macroscopic fuel cell behaviors.

CRediT authorship contribution statement

Marc Ayoub: Writing – original draft, Visualization, Resources, Project administration, Methodology, Investigation, Data curation, Conceptualization. **Christoph Hübner:** Writing – review & editing. **Philipp Martschin:** Writing – review & editing. **Jochen Kerres:** Writing – review & editing, Supervision. **Simon Thiele:** Writing – review & editing, Supervision, Funding acquisition. **Matthew Brodt:** Writing – review & editing, Resources, Project administration, Methodology, Conceptualization.

Declaration of competing interest

The authors declare that they have no known competing financial interests or personal relationships that could have appeared to influence the work reported in this paper.

Acknowledgments

We gratefully express our gratitude to 3 M™ for providing the ionomer for this study.

Appendix A. Supplementary data

Supplementary data to this article can be found online at https://doi.org/10.1016/j.ijhydene.2025.05.107.

References

[1] Orfanidi A, Rheinländer PJ, Schulte N, Gasteiger HA. Ink solvent dependence of the ionomer distribution in the catalyst layer of a PEMFC. J Electrochem Soc 2018;165(14):F1254–63. https://doi.org/10.1149/2.1251814jes.
[2] Balu R, et al. Evolution of the interfacial structure of a catalyst ink with the quality of the dispersing solvent: a contrast variation small-angle and ultrasmall-angle neutron scattering investigation. ACS Appl Mater Interfaces 2019;11(10):9934–46. https://doi.org/10.1021/acsami.8b20645.
[3] Guo Y, et al. The controllable design of catalyst inks to enhance PEMFC performance: a review. Electrochem Energy Rev 2021;4(1):67–100. https://doi.org/10.1007/s41918-020-00083-2 (in En;en).
[4] Mabuchi T, Huang S-F, Tokumasu T. Dispersion of Nafion ionomer aggregates in 1-propanol/water solutions: effects of ionomer concentration, alcohol content, and salt addition. Macromolecules 2020;53(9):3273–83. https://doi.org/10.1021/acs.macromol.9b02725.
[5] Moore RB, Martin CR. Chemical and morphological properties of solution-cast perfluorosulfonate ionomers. Macromolecules 1988;21(5):1334–9. https://doi.org/10.1021/ma00183a025.
[6] Tarokh A, Karan K, Ponnurangam S. Atomistic MD study of Nafion dispersions: role of solvent and counterion in the aggregate structure, ionic clustering, and acid dissociation. Macromolecules 2020;53(1):288–301. https://doi.org/10.1021/acs.macromol.9b01663.
[7] van Cleve T, et al. Dictating Pt-based electrocatalyst performance in polymer electrolyte fuel cells, from formulation to application. ACS Appl Mater Interfaces 2019;11(50):46953–64. https://doi.org/10.1021/acsami.9b17614.
[8] Mauger SA, et al. Influence of ink formulation and drying conditions on ionomer distribution in high-performance roll-to-roll-coated gas-diffusion electrodes. Meet Abstr 2020;(34):2218. https://doi.org/10.1149/MA2020-02342218mtgabs. MA2020-02.
[9] Kim T-H, Yi J-Y, Jung C-Y, Jeong E, Yi S-C. Solvent effect on the Nafion agglomerate morphology in the catalyst layer of the proton exchange membrane fuel cells. Int J Hydrogen Energy 2017;42(1):478–85. https://doi.org/10.1016/j.ijhydene.2016.12.015.
[10] Lauf P, et al. Be aware of the effect of electrode activation and morphology on its performance in gas diffusion electrode setups. J Power Sources 2024;623:235352. https://doi.org/10.1016/j.jpowsour.2024.235352.
[11] Ngo TT, Yu TL, Lin H-L. Influence of the composition of isopropyl alcohol/water mixture solvents in catalyst ink solutions on proton exchange membrane fuel cell performance. J Power Sources 2013;225:293–303. https://doi.org/10.1016/j.jpowsour.2012.10.055.
[12] Gong Q, et al. Effects of ink formulation on construction of catalyst layers for high-performance polymer electrolyte membrane fuel cells. ACS Appl Mater Interfaces 2021;13(31):37004–13. https://doi.org/10.1021/acsami.1c06711.
[13] Liu H, Ney L, Zamel N, Li X. Effect of catalyst ink and formation process on the multiscale structure of catalyst layers in PEM fuel cells. Appl Sci 2022;12(8):3776. https://doi.org/10.3390/app12083776.
[14] Ney L, et al. Screen printing catalyst inks with enhanced process stability for PEM fuel cell production. Fuel Cells 2024. https://doi.org/10.1002/fuce.202400158.
[15] Chisaka M, Matsuoka E, Daiguji H. Effect of organic solvents on the pore structure of catalyst layers in polymer electrolyte membrane fuel cells. J Electrochem Soc 2010;157(8):B1218. https://doi.org/10.1149/1.3439617.
[16] Mashio T, Ohma A, Tokumasu T. Molecular dynamics study of ionomer adsorption at a carbon surface in catalyst ink. Electrochim Acta 2016;202:14–23. https://doi.org/10.1016/j.electacta.2016.04.004.
[17] Ulsh MPI, Presenter Mauger SA. Material-Process-Performance Relationships in Polymer Electrolyte Membrane Catalyst Inks and Coated Layers [Online]. Available: https://www.hydrogen.energy.gov/library/amr-presentation-database?page=11; 2020.
[18] Medina S, Wang M, Dzara M, Mauger SA, Ulsh M, Pylypenko S. Multi-Technique characterization of gas diffusion fuel cell electrodes. Meet Abstr 2020;(33):2144. https://doi.org/10.1149/MA2020-02332144mtgabs. MA2020-02.
[19] Medina S, et al. Multi-technique characterization of spray coated and roll-to-roll coated gas diffusion fuel cell electrodes. J Power Sources 2023;560:232670. https://doi.org/10.1016/j.jpowsour.2023.232670.
[20] Novy MHL. Structure-Morphology-Property Relationships in Perfluorosulfonic Acid Ionomer Dispersions, Membranes, and Thin Films to Advance Hydrogen Fuel Cell Applications [Online]. Available: https://vtechworks.lib.vt.edu/items/15b2a7a8-26af-4671-8b02-b484bd180c38; 2022.
[21] Hoffmann E, et al. Impact of DAA/water composition on PFSA ionomer conformation. J Colloid Interface Sci 2021;582:883–93. https://doi.org/10.1016/j.jcis.2020.08.058. Pt B.
[22] Khandavalli S, et al. Effect of dispersion medium composition and ionomer concentration on the microstructure and rheology of Fe-N-C platinum group metal-free catalyst inks for polymer electrolyte membrane fuel cells. Langmuir : The ACS J Surf. Colloids 2020;36(41):12247–60. https://doi.org/10.1021/acs.langmuir.0c02015.
[23] Ayoub M, et al. Continuous graded catalyst layers for PEM fuel cells with improved humidity range tolerance. J Electrochem Soc 2024;171(11):114503. https://doi.org/10.1149/1945-7111/ad8d81.
[24] Zhang J, Zhang H, Wu J, Zhang J. Chapter 3 - techniques for PEM fuel cell testing and diagnosis. In: Zhang J, Zhang H, Wu J, Zhang J, editors. Pem fuel cell testing and diagnosis. Amsterdam: Elsevier; 2013. p. 81–119 [Online]. Available: https://www.sciencedirect.com/science/article/pii/B9780444536884000036.
[25] Wang H, Yuan X-Z, Li H, editors. PEM fuel cell diagnostic tools: linear sweep voltammetry. Boca Raton, London, New York: CRC Press; 2011 [Online]. Available: https://www.taylorfrancis.com/books/9780429106255.
[26] Murthy Mahesh, Nicholas T, Sisofo Lii, Baczkowki Carol A. Method and device to improve operation of a fuel cell. Aug 3, 2006. WO2006081009A2.
[27] Makharia R, Mathias MF, Baker DR. Measurement of catalyst layer electrolyte resistance in PEFCs using electrochemical impedance spectroscopy. J Electrochem Soc 2005;152(5):A970. https://doi.org/10.1149/1.1888367.
[28] Murbach M, Gerwe B, Dawson-Elli N, Tsui L. impedance.py: a Python package for electrochemical impedance analysis. JOSS 2020;5(52):2349. https://doi.org/10.21105/joss.02349.
[29] Liu Y, et al. Proton conduction and oxygen reduction kinetics in PEM fuel cell cathodes: effects of ionomer-to-carbon ratio and relative humidity. J Electrochem Soc 2009;156(8):B970. https://doi.org/10.1149/1.3143965.
[30] Neyerlin KC, Gu W, Jorne J, Clark A, Gasteiger HA. Cathode catalyst utilization for the ORR in a PEMFC. J Electrochem Soc 2007;154(2):B279. https://doi.org/10.1149/1.2400626.
[31] Harzer GS. Boosting High Current Density Performance of Durable, Low Pt-Loaded PEM Fuel Cells. Technische Universität München; 2018. https://mediatum.ub.tum.de/1449542.
[32] Baker DR, Caulk DA, Neyerlin KC, Murphy MW. Measurement of oxygen transport resistance in PEM fuel cells by limiting current methods. J Electrochem Soc 2009;156(9):B991. https://doi.org/10.1149/1.3152226.
[33] Mehrazi S, Homayouni T, Kakati N, Sarker M, Rolfe P, Chuang P-YA. A Rheo-Impedance investigation on the interparticle interactions in the catalyst ink and its

impact on electrode network formation in a proton exchange membrane fuel cell. Appl Energy 2024;359:122680. https://doi.org/10.1016/j.apenergy.2024.122680.
[34] Aldebert P, Dreyfus B, Gebel G, Nakamura N, Pineri M, Volino F. Rod like micellar structures in perfluorinated ionomer solutions. J Phys France 1988;49(12):2101–9. https://doi.org/10.1051/jphys:0198800490120210100.
[35] Aldebert P, Dreyfus B, Pineri M. Small-angle neutron scattering of perfluorosulfonated ionomers in solution. Macromolecules 1986;19(10):2651–3. https://doi.org/10.1021/ma00164a035.
[36] Loppinet B, Gebel G, Williams CE. Small-angle scattering study of perfluorosulfonated ionomer solutions. J Phys Chem B 1997;101(10):1884–92. https://doi.org/10.1021/jp9623047.
[37] Szajdzinska-Pietek E, Schlick S, Plonka A. Self-assembling of perfluorinated polymeric surfactants in nonaqueous solvents. Electron spin resonance spectra of nitroxide spin probes in nafion solutions and swollen membranes. Langmuir 1994; 10(7):2188–96. https://doi.org/10.1021/la00019a026.
[38] Nonoyama N, Okazaki S, Weber AZ, Ikogi Y, Yoshida T. Analysis of oxygen-transport diffusion resistance in proton-exchange-membrane fuel cells. J Electrochem Soc 2011;158(4):B416. https://doi.org/10.1149/1.3546038.
[39] Della Bella RKF, Stühmeier BM, Gasteiger HA. Universal correlation between cathode roughness factor and H 2/air performance losses in voltage cycling-based accelerated stress tests. J Electrochem Soc 2022;169(4):44528. https://doi.org/10.1149/1945-7111/ac67b8.